Available online at www.sciencedirect.com
SCIENCE DIRECT
Journal of Controlled Release 111 (2006) 174–184
journal of controlled release
www.elsevier.com/locate/jconrel

# Electron spin resonance microscopy applied to the study of controlled drug release

Aharon Blank [a,1], Jack H. Freed [a,*], Naraharisetti Pavan Kumar [b], Chi-Hwa Wang [b]

[a] National Biomedical Center for Advanced ESR Technology, Department of Chemistry and Chemical Biology, B-52 Baker Laboratory, Cornell University, Ithaca, NY, 14853, USA
[b] Department of Chemical and Biomolecular Engineering, National University of Singapore, Singapore

Received 12 August 2005; accepted 3 November 2005

**Abstract**

We describe our recent developments towards 3D micron-scale imaging capability, based on electron spin resonance (ESR), and its application to the study of controlled release. The method, termed ESR microscopy (ESRM), is an extension of the conventional "millimeter-scale" ESR imaging technique. It employs paramagnetic molecules (such as stable radicals or spin-labeled drugs) and may enable one to obtain accurate 3D spatially resolved information about the drug concentration, its self-diffusion tensor, rotational correlation time and the pH in the release matrix. Theoretical calculations, along with initial experimental results, suggest that a 3D resolution of ~1 μm is feasible with this method. Here we were able to image successfully a high spin concentration sample with a resolution of ~3×3×8 μm and subsequently study a single ~120 μm biodegradable microsphere, internalized with a dilute solution of trityl radical, with a resolution of ~12.7×13.2×26 μm. Analysis of the microsphere ESR imaging data revealed a likely increase in the viscosity inside the sphere and/or binding of the radical molecule to the sphere matrix. Future directions for progress are also discussed.


*Keywords:* ESR imaging; EPR; ESRM; Biodegradable microspheres

## 1. Introduction

The most common method for analyzing controlled drug release from a biodegradable matrix is the in-vitro release test. Such a test involves the insertion of the release matrix into an appropriate liquid solution and then monitoring the time-resolved concentration of the drug in the solution. The in-vitro release test, however, does not provide sufficient information to help support the development of new release matrixes and processes. For that purpose, one would like to have knowledge about the time-resolved drug distribution inside the matrix, erosion of the release matrix, water absorption, matrix swelling, drug diffusion inside the matrix, and other physical and chemical conditions of relevance. To answer these questions, a variety of imaging methods have been developed and employed in recent years to aid the field of controlled drug release. For example, laser scanning confocal fluorescence microscopy (LSCFM) and microfocus X-ray imaging were used to determine the drug spatial distribution within the release matrix [1,2]. Fluorescence resonance energy transfer (FRET) microscopy yielded spatially resolved information about the drug stability during and after the release process [3]; LSCFM and electron spin resonance imaging (ESRI) showed a capability to map the pH and the water diffusion inside the release matrix [4,5]; magnetic resonance imaging (MRI) was used to measure the water diffusion coefficient inside the release matrix and investigated phenomena such as hydration, swelling and porosity [6]; and Fourier transform infrared microscopy (FTIRM) was shown to be a useful analytical tool for the characterization of drug delivery systems [7,8], through its "chemical photography" capability.

In spite of this wide arsenal of methods and tools, there are still several open issues in the field of controlled release, for

* Corresponding author. Tel.: +1 607 255 3647; fax: +1 607 255 6969.
*E-mail address:* jhf3@cornell.edu (J.H. Freed).
[1] Present address: Department of Chemistry, Technion, Haifa, 32000, Israel.

0168-3659/$ - see front matter © 2005 Elsevier B.V. All rights reserved.
doi:10.1016/j.jconrel.2005.11.019

which none of these advanced imaging methods can provide an adequate answer, especially when micron-scale release systems are considered. One such open issue is the need for imaging of the 3D self-diffusion tensor, **D**, of the drug molecule inside the release matrix. In principle, MRI should have the capability to measure such a property [9]. In practice, however, due to signal-to-noise-ratio (SNR) limitations, MRI can in most cases measure only the diffusion coefficient of the water in the matrix and not the **D** of the drug molecule itself, whose concentration is often ~4–5 orders of magnitude smaller than that of the water. Such a limitation is even more severe when microscopic release systems are considered (as in the case of microspheres), where the entire size of the system is ~100 μm. This size approaches the resolution limits of NMR microscopy for water-based samples (~10–20 μm) [10], implying that SNR limitations will prohibit drug molecule NMR imaging in these systems. Another potential method to image the drug diffusion may be through fluorescence recovery after photobleaching (FRAP) [11]. In practice, however, this method cannot be used for most drug release systems due to their nanoscopic porous nature, which implies a restricted diffusion phenomenon (while the FRAP method is based on the assumption of a homogenous medium to extract **D** out of its measured data). In addition, the FRAP technique cannot differentiate the tensorial nature of **D** (and obtains only a scalar average-like diffusion parameter $D=\mathrm{trace}(\mathbf{D})$).

An additional dynamic parameter of importance, which can provide information about the state of the drug in the matrix, is the rotational correlation time, $\tau_c$, of the drug molecule. Thus, for example, if one measures a relatively short rotational correlation time along with measured low or bounded diffusion, it may imply that the drug molecules are not bound to the matrix but are nevertheless caught in small pores. Alternatively, for example, one may measure relatively large rotational correlation times, which would imply strong interaction between the drug and the bounding matrix. As in the previous example, in principle, NMR [12] and fluorescence depolarization method [13] should be useful for imaging $\tau_c$ of the drug inside the matrix. In practice, both methods are limited to a rather long (ns and above) rotational correlation times; the NMR method is often not sensitive enough (as described above) and the optical method requires a-priori knowledge of many parameters to accurately determine $\tau_c$.

Even with respect to the fundamental quantity of the 3D time-resolved spatial distribution (concentration) of the drug inside the release matrix, there is still a wide gap between the needed and the available imaging means. Thus, in many cases, one cannot measure properly the 3D drug distribution by any of the conventional imaging methods described above. For example, fluorescence methods looking at fluorescent-labeled drugs often find it difficult to image the release matrix at high resolution without removing it from the release in-vitro chamber. More importantly, frequently the release matrix is opaque and prevents one from obtaining information from within the sphere. Finally, even if some light does penetrate through the matrix and an image is obtained, it cannot be calibrated, due to unknown absorption and scattering phenomena that affect the signal amplitude from the internal voxels of the release matrix. Near infrared (NIR), mid infrared (MIR) and Raman imaging have been used to study the distribution of chemical species within pharmaceutical products at maximum resolution of ~5 μm [7,8,14]. However, when used in transmittance mode, MIR imaging requires the sample to be sectioned to ~10 μm thick slices and, like Raman imaging, requires the sample to be optically flat. NIR imaging, in diffuse reflectance mode, does not require sample sectioning or an optically flat sample, but unfortunately it can only be used to study the surface of a sample since it penetrates to a relatively shallow depth. In addition to these problems, when there is spectral overlap between the active drug and other inert ingredients, complex statistical analyses that are open to error are required to attempt to distinguish the various components of the mixture. Microfocused X-ray imaging can overcome some of these drawbacks of optical methods and the sensitivity problems of NMR, but it is limited to specific type of drugs (that provide sufficient X-ray contrast) and has limited spatial resolution of several tens of microns [2].

Here we shall present a new method aimed at 3D imaging with high resolution of the relevant parameters of interest described above. The imaging method is based on electron spin resonance (ESR). ESR imaging (ESRI) is conceptually very similar to MRI, but observes the signal of paramagnetic molecules rather than that of the nuclei employed in NMR. ESRI has already proven capabilities of providing important information about controlled drug release systems, both in vitro [15] and in vivo [16]. As in the case of fluorescence imaging, one is required to attach a label to the molecule of interest to facilitate its observation by ESR. These paramagnetic labels (often from the nitroxide family) are much smaller than the fluorescence probes and can be attached to a large class of molecules [17]. In ESR, obtaining the physical and chemical information of interest is often based on the sensitivity of the ESR spectrum of nitroxides to their environment. For, example, the rotational correlation time, $\tau_c$, of nitroxide-labeled molecules is determined from the line shape of their ESR spectra, and this property has been employed to characterize the environment in solid and liquid crystalline phases such as biological membranes, liposomes and macroporous polymeric resins [18,19]. This methodology was also applied to probe the morphology of hydrogels and polymer–polymer blends [20]. Furthermore, the measurements of microviscosity and pH (using specially designed nitroxides) has been used to characterize the environment to which drugs are exposed prior to their release from biodegradable polymers [16,21]. These past examples, employing not only conventional spectroscopy, but also spatially resolved spectroscopy (in the 0.2–1 mm resolution scale), clearly showed that ESR is a powerful nondestructive tool for studying in detail the internal structure, mobility and hydration properties of various polymeric matrix systems, including the one employed in controlled drug release process.

Recently, we have been aiming at extending the capabilities of conventional "millimeter-scale" ESRI to the realm of microscopic resolution [22–24]. This new micro-imaging method, termed ESR microscopy (ESRM), has the potential

of adding the missing feature, namely high 3D spatial resolution that limited many of the previous ESR and ESRI studies. This paper will describe the current experimental capabilities and the future possibilities of ESRM. It will also provide initial experimental evidence for the feasibility of ESRM to provide valuable physical information at high spatial resolution in the field of controlled drug release through the use of biodegradable microspheres as a model system.

## 2. Methods, instrumentation and materials

### 2.1. Methods and instrumentation

#### 2.1.1. CW ESR spectrometer

As a preliminary stage of the experimental protocol, we often examine our samples with a conventional commercial continuous wave (CW) ESR spectrometer (9 GHz EMX system, from Bruker, Germany). These measurements are carried out in a rectangular $TE_{102}$ mode cavity, where the aqueous samples are placed in a thin glass capillary tube (i.d. 1 mm, o.d. 1.8 mm), which are degassed in a vacuum line and sealed (to eliminate the presence of the paramagnetic $O_2$). In the present work, the CW ESR experiments provided positive identification of the radicals in the sample, they showed a unique line shape for various parts of the sample (see below), and they also enabled time-resolved measurements of the total radical concentration in the water phase of the sample, which were used to estimate the release kinetic rates.

#### 2.1.2. The ESRM method

Magnetic resonance (MR) microscopy (employing NMR or ESR) can be conceptually visualized as a scaled down version of the common "large-scale" MR imaging methods used with humans and animals. Thus, while MR images are most commonly obtained employing objects that are on the 10–100 cm length scale, with a resolution of ~1–10 mm, MR microscopy involves objects that are on the 0.1–1 mm length scale, with a resolution of ~1–10 μm [9,24]. The increased resolution is achieved by the use of small excitation and detection probes, combined with strong and efficient magnetic field gradient coils. Since NMR and ESR imaging have very similar physical principles and measure similar parameters, the legitimate question that immediately comes into play is why should one pursue the less advanced ESRM technique over the more common NMR methodology? ESR has inherently several potential virtues over NMR, which could make this technique more suitable for microscopic applications. For example, the signal per spin is much higher than in NMR [25], diffusion does not limit the resolution in the short time scales (spin–spin relaxation time, $T_2$'s ~ μs) of the ESR measurements [26–28], and ESR micro-resonators detect with a quality factor ($Q$) of ~1000 compared to the $Q$ ~ 10 of the NMR micro-coils [9,29]. These advantages lead to the potential for sub-micron-scale resolution with 1 mM electron spin concentration [22], compared to a practical limit of ~10 μm resolution with ~100 M proton concentration in NMR microscopy [10]. The capability to obtain high resolution images of a sample with low molecular concentration (spins in our case) is of crucial importance in controlled drug delivery research. In addition to the sensitivity and the resolution advantages, one should also note that the ESR line shape is more sensitive to dynamic effects, leading to greater information content [30,31], and finally the low cost of ESR electromagnets compared to the expensive NMR superconducting magnets is important for the wide dissemination of this technique. Since most samples do not contain unpaired electrons (e.g. stable free radicals), these paramagnetic species must be added in a manner similar to that of adding contrast agents in NMR or dyes in optics. This is a standard procedure, especially for microscopy of controlled drug release, when the drug is often labeled with an appropriate marker.

#### 2.1.3. The ESRM system

Here we will briefly describe the pulsed ESRM system employed in the current study. An earlier version, employing a 9 GHz imaging probe, was presented recently [24]. Fig. 1 shows the overall block diagram of the ESRM system. The system is built from the following main modules: (a) Standard PC that controls the image acquisition process through the user interface software (LabView from National Instruments). (b) Timing system (PCI card PulseBlaster Model 100-24, SpinCore), which has 24 TTL outputs, time resolution of 10 ns, programming time of ~10 μs and minimal pulse length of 50 ns. The timing system triggers the microwave (MW) and gradient pulses, determines the phase of the transmitted MW pulses through a bi-phase modulator and an 8-bit phase shifter located in the MW bridge (see below), and provides triggers for the protection switch of the sensitive receiver while the high power MW pulses are transmitted. (c) An 8-bit PCI-format digitizer card for raw data acquisition and averaging (AP-240, Acqiris), which has two channels, a sampling rate of 1 GHz, capability of averaging up to 1 M waveforms/s, and has memory depth of 1 Mbyte. This card is used to acquire the ESR signal. (d) PCI analog output card with four outputs (PCI-6711, National Instruments). This card is used to determine the amplitude of the magnetic field gradients for the three imaging axes. (e) Synthesized microwave reference source (HP 8672A) with power output of 10 dBm in the 2–18 GHz range, controlled by a PCI-GPIB card ($n$) in the PC (GPIB card from Measurement

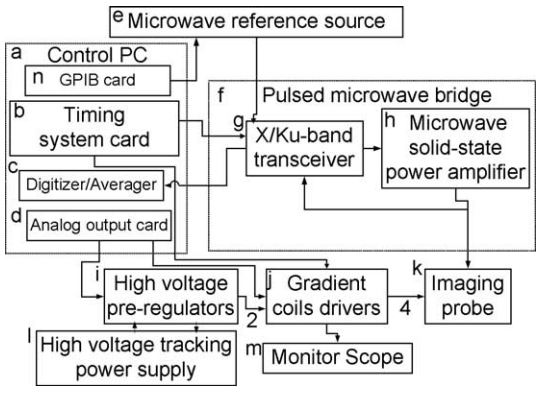


Fig. 1. Block diagram of the pulsed ESR microscopy system.

Computing). (f) A "home-built" pulsed microwave bridge containing a 6–17 GHz low power transceiver (g) and a solid-state power amplifier (h) with ~2 W output and gain of >40 dB (Quinstar). The relatively low power output of the transceiver is sufficient to provide 90° pulses of ~40–60 ns (depending on frequency) with the small resonator we employ [24]. The homodyne MW transceiver incorporates a single transmission channel with a fast (~10 ns settling time) bi-phase modulator, which controls the individual MW pulse phase (e.g. phase of 0° or 180° for spin echo phase cycling). In addition to the bi-phase modulator, the transmit channel also includes a slower (500 ns settling time) 8-bit digital phase shifter (for more involved phase cycling schemes of the entire pulse sequence). The pulse imaging probe (k) was described in detail in [23,24] in the framework of 9 GHz CW and pulse research. In the present studies, the diameter of the resonator was reduced from 2.31 to 1.4 mm to increase the resonance frequency from 9 to 16 GHz (thereby improving sensitivity). The *x*- and *y*-axes pulsed gradient coils in the imaging probe are driven by a pair of "home-built" gradient coil drivers (j) fed by a "home-built" pre-regulated high voltage power supply (HVPR). These two channels can generate high (up to ~8 A peak) half-sine current pulses by pre-charging a capacitor and subsequently discharging it into the gradient coil [32]. The capacitor voltage is determined by the HVPR and is proportional to the analog voltage the HVPR receives from the analog-output card (d). In addition to these two pulsed channels of the gradient coils driver, there are two more channels that produce constant DC current. The DC current of one channel goes into the gradient coil, which spatially encodes the information of the sample *z*-axis and the second DC channel goes into a bias coil. The bias coil produces a DC magnetic field that is added to the main static field of the electromagnet. The magnitude of the small added DC field is controlled by the computer and is used to lock the total magnetic field on the resonance field of the spins by occasionally sampling the free induction decay (FID) signal without any gradients and correcting for any field drifts of the large electromagnet [23].

The performance of the system in terms of resolution and SNR were evaluated through the use of test samples. Fig. 2 shows an example of an ESR image of a test sample containing solid lithium phthalocyanine (LiPc) crystals, which is a common stable solid free radical [33]. The image was obtained through the use of the pulse sequence shown in Fig. 3. The ESR image acquisition time was 25 min with a measured resolution of ~3×3×8 μm. The image contains 180×180×128 voxels and the single voxel SNR is ~550. These values represent the high end of the current system capabilities, for a relatively high

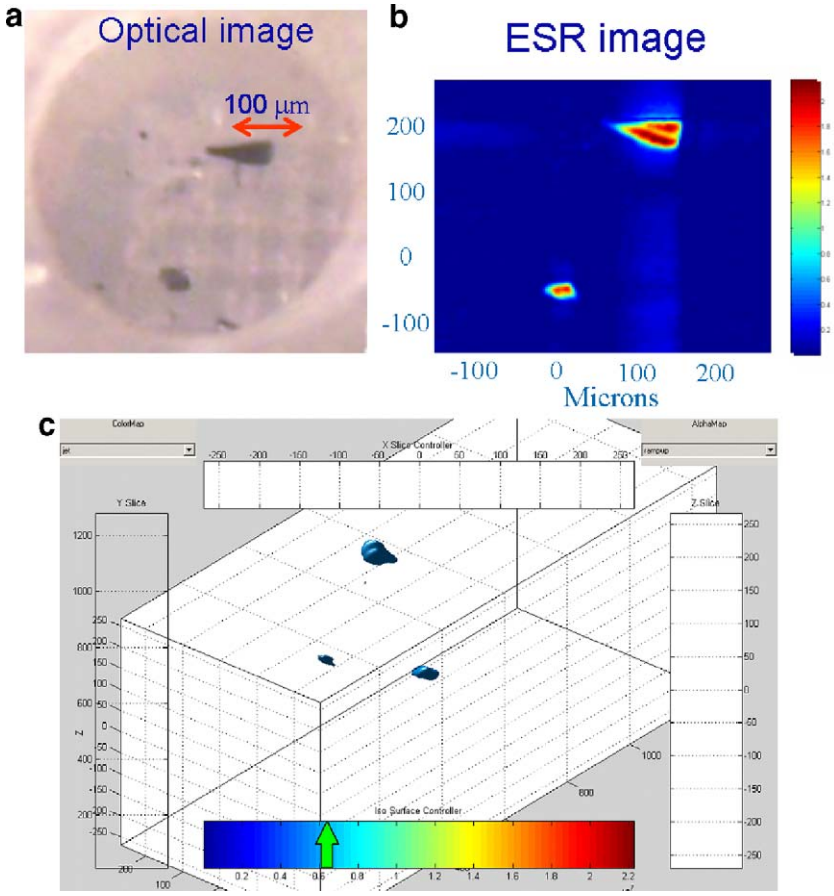


Fig. 2. Optical and ESR images of a test sample made of three small crystals of LiPc. (a) An optical image of the crystals shown through the hole in the cylindrical dielectric resonator we employ [24] (the third crystal is partially hidden). (b) A 2D cut of the 3D ESR image obtained at 16 GHz. The vertical color bar represents the relative pixel ESR signal in arbitrary linear units. (c) 3D object reconstruction based on the 3D ESR image data. (The third, smallest crystal is positioned at a different *z* plane and thus not apparent in the 2D cut but can be seen in the full 3D data.)

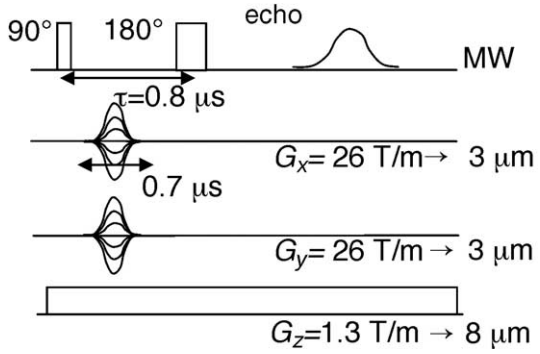


Fig. 3. Imaging pulse sequence employed for the acquisition of the data shown in Fig. 2. Phase gradients are employed for spatially encoding the *x*- and *y*-axes of the sample, while a constant gradient is used along the *z*-axis. Typical peak values of the pulsed ($G_x$, $G_y$) and the constant ($G_z$) field gradients with the corresponding resolution are shown (see also [22,24] for more details).

spin concentration samples (the LiPc crystals contain $\sim 10^8$ spins per $[1\ \mu m]^3$ [24]). For other applications, however, including controlled drug release, one should expect to encounter concentration levels on the order of 1mM (or $\sim 6\times 10^5$ spins per $[1\ \mu m]^3$). At that level of concentration, the SNR and the resolution are degraded with respect to the LiPc samples. A typical representative ESR image for the case of relatively low spin concentration is given in Fig. 4. The image resolution is $\sim 7\times 7\times 12$ μm and the single voxel SNR is ~30 leading to well-resolved 3D compartments within the small nylon mesh. This image contains $256\times 256\times 128$ voxels, with $\sim 3\times 10^8$ spins per voxel.

The unique trityl and LiPc probes may be used for many of the applications described above. Nevertheless, one may argue that the most common probes today, especially for spin labeling, are still based on the nitroxide family, and thus we consider the prospects of employing such probes in high resolution ESRM. Basically, nitroxides exhibit a wide range of lineshapes and relaxation times, depending on the local environment, resonant field and frequency, and nitroxide type [30]. It is clear that, for ESRM purposes, one should prefer $^{15}$N-labeled deuterated nitroxides. These radicals are characterized by relatively narrow lines (for example ~0.16 G for PD TEMPONE), for low viscosity media. Let us consider pulse imaging experiments and provide some quantitative comparison between nitroxides and protonated trityl. In principle image resolution can be degraded due to SNR reduction, which is a fundamental physical limitation, and/or lower gradient effectiveness for wide lines/short relaxation times, which largely is a technical challenge. In terms of SNR, a decrease in $T_2$ from 1 μs (typical of trityl in the presence of some $O_2$) to 0.1 μs (i.e. quite restricted motion of nitroxide probes) will require a corresponding increase in the bandwidth of acquisition by a factor of 10. This will result in an

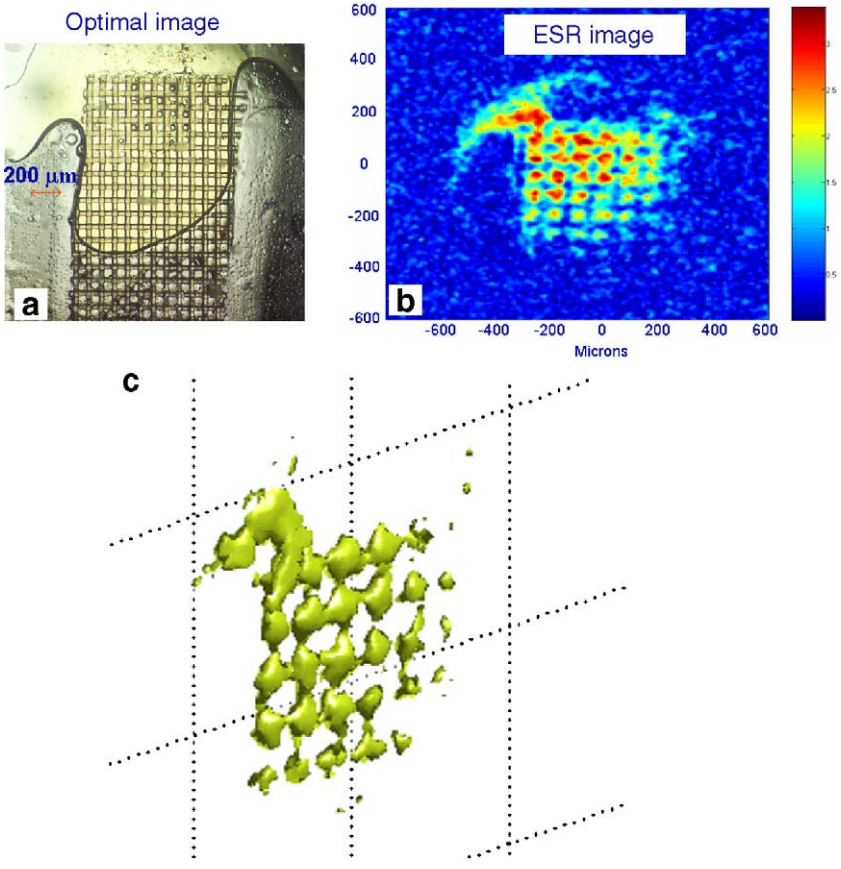


Fig. 4. Optical and ESR images of a test sample made of 1 mM trityl radical water solution [36] embedded in a woven Nylon mesh with mesh aperture of $50\times 50$ μm and wire diameter of 39 μm (Goodfellow, USA). (a) An optical image of the solution and the mesh prior to measuring the ESR image. (b) A 2D cut of the 3D ESR image obtained at 16 GHz. The vertical color bar represents the relative pixel ESR signal in arbitrary linear units. (c) 3D object reconstruction based on the 3D ESR image data. The discrepancies between the ESR image and the optical image are due to sample dehydration during the ESR measurements.

SNR reduction by a factor of ~3.3, which must be multiplied by 2 (2 lines for $^{15}N$ nitroxide vs. 1 of the trityl). However, the fundamental SNR limitation of the 3D resolution with respect to a linear dimension will be degraded by just a factor of $(6.6)^{1/3} \sim 1.9$, for such a large decrease in $T_2$ (keeping the imaging time constant). The challenge in this case is therefore not the fundamental SNR limit but rather the technical aspect of dealing with $T_2$'s of the order of 100–200 ns, which requires short dead times and short pulsed field gradients. Nevertheless, based on the work performed to-date in the field of pulse ESR [31] and ESRM, this is within our projected technological capabilities.

### 2.2. Materials

Poly(D,L-lactic-*co*-glycolic acid 50:50) with molecular weight of 40,000–75,000 (termed here PLGA), poly(ethylene glycol) with molecular weight of 8000 (termed PEG) and poly (vinylalcohol) with molecular weight of 30,000–70,000 (PVA) were all purchased from Sigma-Aldrich (St. Louis, USA). Dichloromethane (HPLC grade) was obtained from Tedia (Fairfield, OH, USA). Trityl radical (tris-(8-carboxyl-2,2,6,6-tetrakis-methyl-benzo[1,2*d*:4,5-*d*′]bis(1,3)dithiole)methyl, Fig. 5) was obtained from Nycomed Innovations (Sweden).

### 2.3. Sample preparation

#### 2.3.1. The biodegradable microspheres

A 500 ml solution of 2% (w/v) PVA in water was prepared for the solvent evaporation method [34,35] while bubbling $N_2$ through the liquid to remove the dissolved oxygen for 2 h. A 200 mg mixture of PLGA and PEG in a varying PLGA/PEG ratio (several samples with different ratios were prepared, ranging from 0% to 10% by weight) was added to 2 ml of dichloromethane. Subsequently, the trityl radical solution in water (2 mg/100 μl) was added to the dichloromethane–polymer solution. The mixture was sonicated (sonication probe, model VCX750, Vibracell Sonics, Sonics and Materials Inc., CT, USA) at a power of 150 W for 30 s (15 s, twice) and then poured into the PVA solution while stirring at 500 rpm with a magnetic stirrer. The stirring continued for 4 h, under $N_2$ atmosphere in the dark, until all the dichloromethane was evaporated. The resultant solution was filtered and the collected microspheres were freeze dried overnight and sealed under $N_2$ atmosphere and stored for later use.

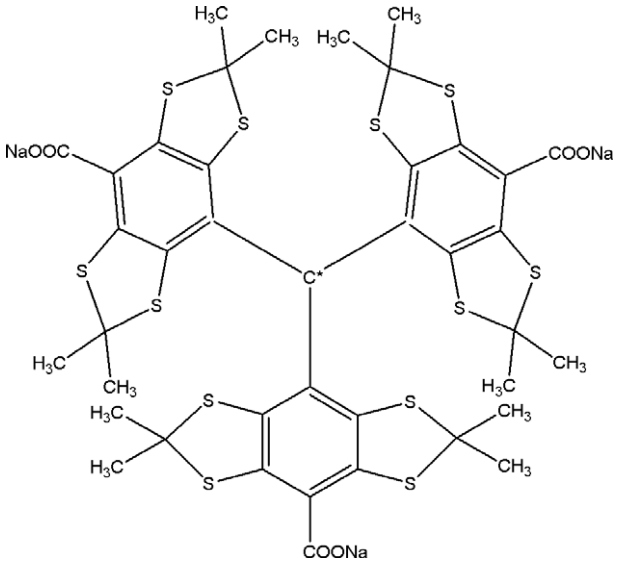


Fig. 5. The trityl radical salt.

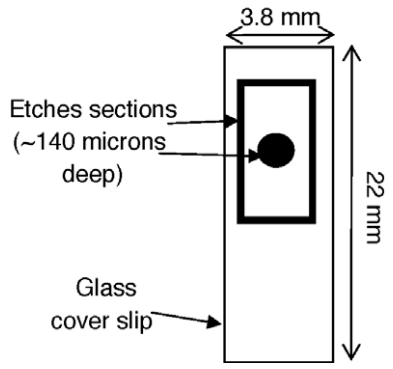


Fig. 6. The glass container used for the ESRM sample preparation.

#### 2.3.2. Samples preparation for the ESR imaging experiment

Thin glass cover slips (~200 μm thick) were cut with a diamond wire saw (Model 4240 Well, Germany) to a 3.8×22 mm rectangular pieces. The rectangular pieces were etched in a Fluosilicic acid 33% (Riedel-de Haën, Germany) bath with a paraffin wax mask to produce the pattern, as shown in Fig. 6. The spheres were picked with fine tweezers and glued to the bottom of the glass container with UV curable glue. A 1 mM trityl solution in water was added to the sample of the spheres under Ar atmosphere. The etched glass with the spheres and the solution was then covered with a similar rectangular glass piece (150 μm thick, without acid etched patterns) and sealed with UV curable glue. The relatively high hygroscopicity of the UV glue resulted in sample drying over a period of 1–3 days, depending on the outside air moisture. To overcome this problem, an additional thin layer of high vacuum silicone sealant (VacSeal from SPI supplies, US) was applied to the glass sample, after the UV glue was cured.

Fig. 7 shows a typical sphere sample after preparation, placed inside the ESRM imaging probe. It should be noted that,

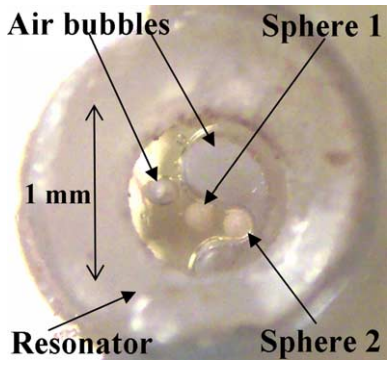


Fig. 7. Sample containing microspheres embedded in 1 mM trityl water solution, placed inside the imaging probe, ready for ESRM experiments.

during sample preparation, one is often encountered with some gas bubbles trapped between the glass slides, as is apparent in the present case. This is normally an unwanted effect, since the bubbles may shift position during the imaging process and future improvements in sample preparation protocol should resolve this problem. However, on the positive side, one can take advantage of these bubbles to identify the various features in the image, as described below.

## 3. Results and discussion

### 3.1. CW ESR

At the preliminary stages of the experiments, we needed to find out the optimal composition of PLGA, PEG and trityl radical that would enable controlled release in the time scale of hours/days. This condition is different from many of the controlled drug release applications, where sustained release of about ~1 month period is required. However, such a long time scale is not practical when the development of new experimental methodology is considered, where mistakes or problems must be identified relatively fast to enable one to converge to a reasonable working methodology. Therefore, the typical time scale of hours/days (after which radical concentration equilibrium is reached between the inner and the outer parts of the sphere) is most appropriate, since, on the one hand, it enables relatively fast iterations with different samples and, on the other hand, it is not too short for the time scale of the ESRM system (which currently requires at least ~30–60 min for data acquisition for each 3D image). Finding the optimal sphere composition that will comply with this release kinetics requirement is not trivial, since the trityl is different from common drugs usually encountered in the context of controlled release processes. Trityl is a relatively small molecule (molecular weight of 1065, Fig. 5), which is highly soluble in water (electrolytic salt). The optimal sphere composition was found by carrying out a series of CW ESR measurements with spheres made of different compositions of polymers (PEG/PLGA ratio of 10% down to 0%) containing the internalized trityl radical. The spheres were placed inside a thin ESR tube (see above) and pure distilled water was added to initiate the release process of the solid trityl radical that is trapped inside the spheres (Fig. 8, on the right). These CW ESR measurements provide mainly the signal from the solvated radical, which can be either inside or outside the spheres (the immobilized solid radical in the spheres, prior to the penetration of water into the sphere, gives rise to a very weak broad signal, see Fig. 8d). The measurements of the PLGA-trityl spheres (0% PEG) revealed that, apart from an initial release of radicals into the water (in the time scale of minutes), the solvated radical signal remained almost constant thereafter. This can be explained if the signal originates only

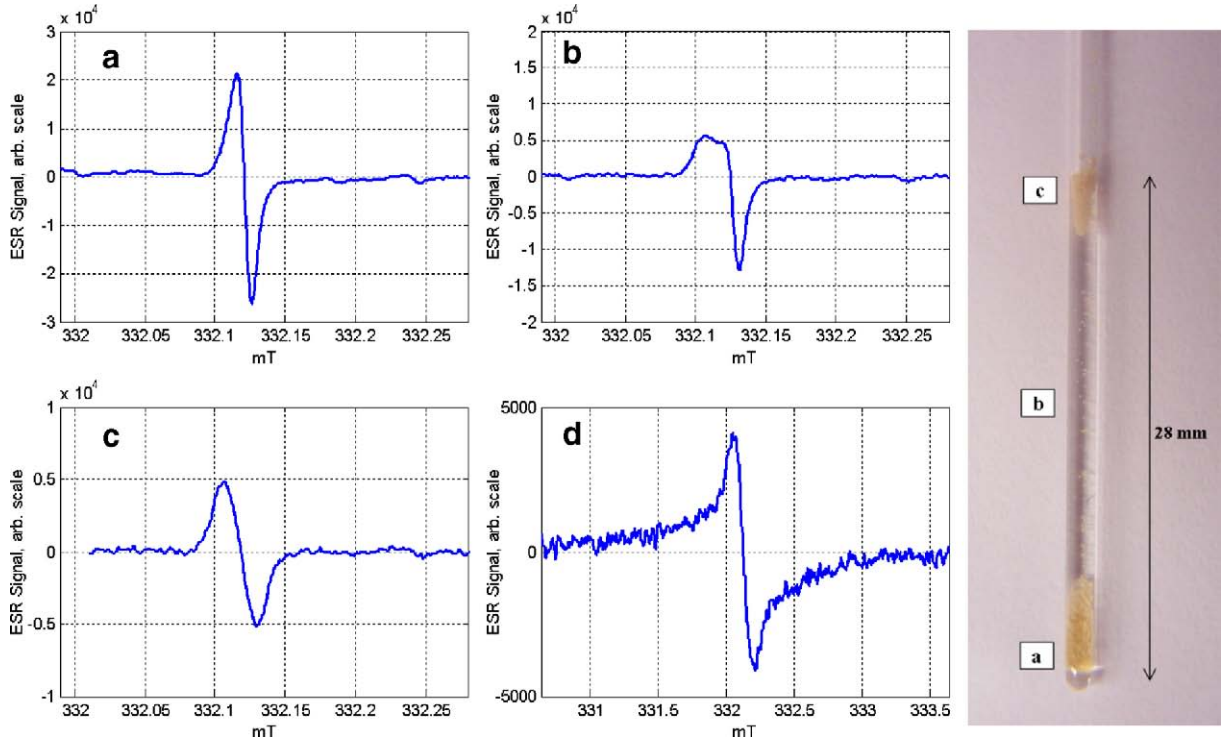


Fig. 8. Typical CW ESR spectra from a sample with spheres made of 0.25% PEG in PLGA, with internalized trityl radical (photo shown on the right). (a) Spectrum acquired when position "a", as shown on the right, is placed at the center of the ESR resonator (Bruker $TE_{102}$ rectangular cavity [25]). The *x*-axis represents the magnetic field in milli-Tesla (mT) and the *y*-axis represents the ESR signal in arbitrary units. The spectrum shows a single sharp (0.01 mT line width) line, typical of deoxygenated trityl solution in water [36,37]. (b) Spectrum acquired when position "b", as shown in on the right, is placed at the center of the ESR resonator. The spectrum shows two components having line width of 0.01 mT and 0.023 mT, with slightly different *g* factor. (c) Spectrum corresponding to location "c" on the right photo, showing single line with line width of ~0.023 mT. (d) Control experiment for measuring the signal of the same quantity of dry spheres. Notice that the signal is much weaker and the linewidth is 0.16 mT (here the magnetic field scan is 3 mT, compared to 0.3 mT in graphs a–c).

from radicals that were about the surface of the spheres and were dissolved and released to the water very fast. Thus, probably in this case of 0% PEG, the bulk radicals inside the spheres were not able to get out and also the water could not penetrate and dissolve them inside the spheres. The probable reason for this is that, without any PEG, the small radical molecules are completely encapsulated by the PLGA and the spheres are produced almost without any percolated pores. This kind of structure slows significantly the release from the bulk of the sphere, since the PLGA degradation by water occurs in a time scale of weeks [1]. At relatively high PEG/PLGA concentration of 1%, 5%, and 10%, the release of radical from within the spheres was in the time scale of tens of minutes. It was finally found that concentrations of 0.5% and 0.25% PEG are most suitable for the present ESRM experiments. These compositions showed typical release kinetics in a time scale ranging from several hours (0.5%) to 1–3 days (0.25%), after which the radical release has ceased almost completely (and thus probably most of the spheres reached equilibrium in terms of radical concentration for the inner and outer media). A representative time-resolved ESR spectrum showing the release kinetics pattern as measured for the 0.5% PEG spheres is given in Fig. 9. It shows how the broader signal from the radical in the spheres is generated rapidly (as water penetrates the spheres) and then gradually transforms into the narrower signal of the free trityl solution (as the trityl is released) over a time scale of several hours. It is thus clear that, as discussed above, the time scale of the release kinetics for this composition is suitable for the ESRM experiments performed here, aiming mainly at methodology development.

Let us consider more carefully the spectral shapes that appear in Figs. 8 and 9, which capture in a qualitative manner the inhomogeneous nature of the examined sample. In Fig. 8a, one can observe the signal from spheres that have absorbed water completely and sunk to the bottom of the tube. The signal from this lower part of the tube should in principle contain two components, one originating from the radical solution inside the spheres and one from the trityl aqueous solution around the spheres (with the radical that was released from the spheres). In practice, however, the lower part of the sample shows only a single component "water-like" spectrum, which is indistinguishable from the common trityl aqueous solution signal [36–38]. This suggests that the spheres on the bottom do not have special interaction with the solvated radicals inside them and probably serve as a simple porous media where the trityl solution flows freely. Contrast to the spheres that are on the bottom of the tube, the spheres that are partially saturated with water (and still float) exhibit different spectrum from that of the aqueous trityl solution. This is apparent in Fig. 8b and c (and also in Fig. 9), where one can clearly see two component spectra, one originating from the supernatant trityl solution and one probably from the trityl aqueous solution inside the spheres. The signal from the trityl solution inside the spheres is broader and has a slightly different g factor. This may suggest that the radicals in those partially water-saturated spheres are still

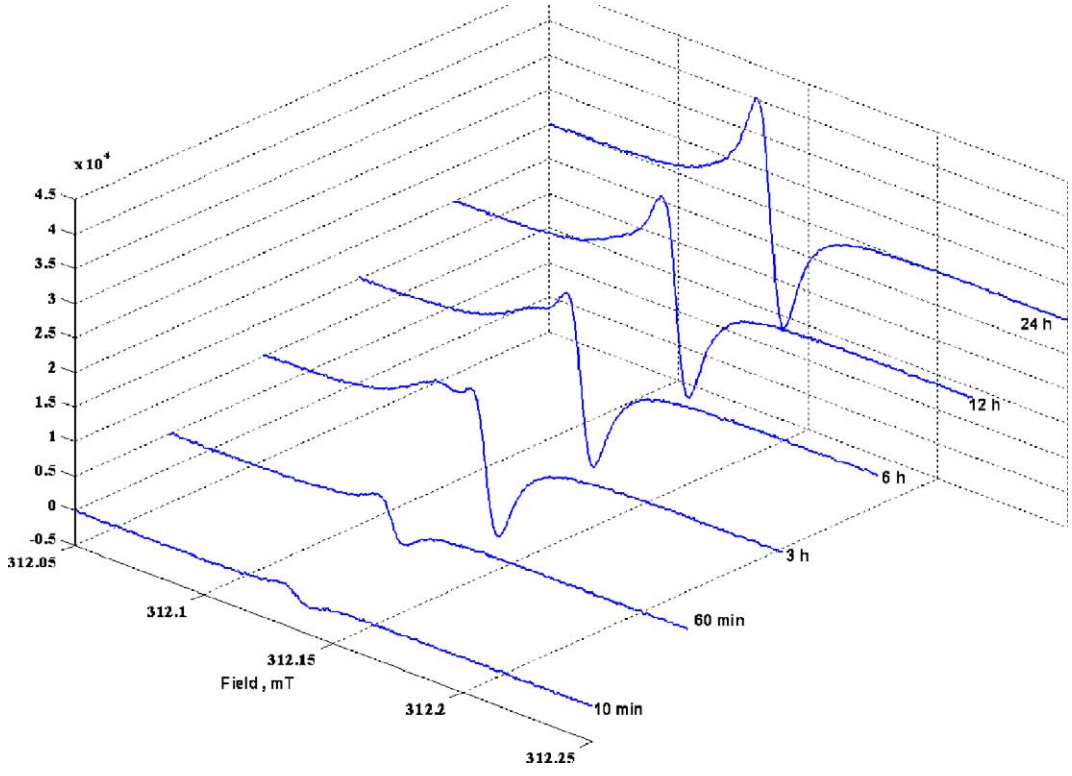


Fig. 9. Time-resolved ESR spectra for trityl embedded in microspheres with 0.5% PEG, immersed in water. The spectra show the contribution from the free trityl in the liquid solution (the narrower line) and the trityl inside the spheres (broader line) that is released almost completely after ~24 h. The time-resolved spectra for the microspheres with other PEG concentrations follow similar pattern, but with different time scales (see text).

slightly bound or have some other interaction with the matrix. This phenomenon can be examined on the micron-scale through ESRM, as we shall see below.

### 3.2. ESRM measurements

It can be concluded that these initial CW experiments showed that the PLGA/PEG/trityl microspheres can be used as a test sample to examine the applicability of ESRM to the field of controlled release imaging. The spheres exhibited release kinetics in the appropriate time scale and showed unique characteristic spectral information from their inner volume. The question that still remained to be answered is whether ESRM can provide high enough SNR and resolution to obtain meaningful and unique physical information in the individual sphere level and below it. In order to answer this question, several microspheres samples embedded in 1 mM water trityl solution were prepared and were subsequently examined by ESRM measurements. A photo of such a sample, inside the 16 GHz ESRM imaging probe, is given in Fig. 7. The reason for employing 1 mM trityl solution to induce the release, instead of pure water (as was done in the CW experiments), is to have a constant reference calibrated signal throughout the measurements. (Due to the small size of the spheres, even if they release all their contents, the trityl concentration in the solution does not change significantly.) This condition is different from what is customary in most in-vitro release experiments, which are most commonly conducted under "perfect-sink" condition. However, since the purpose of the present ESRM experiment is not to examine the release process per-se but mainly to examine the resolution, SNR and the type of information ESRM can provide, this issue is not of great concern at this stage. In the future, one may use different radicals, possibly solid LiPc-type radicals [39,40] as the reference signal source. These radicals do not dissolve in water and therefore would enable sample preparation that provides the "perfect sink condition" for the drug sustained release. Fig. 10a–c show a series of images obtained by ESRM for this sample, at different delay times ($\tau$) between the 90° and 180° pulses (cf. Fig. 3). The 3D ESR image acquisition time was 40 min for each different $\tau$. The image contains $100\times100\times128$ voxels, with a resolution of $\sim12.7\times13.2\times26$ μm. In general, the agreement between the ESR image and the optical image (Fig. 7) is good. In that respect, one must consider the fact that the ESR signal is collected mainly from the central part of the resonator (~0.8 mm diameter) and also that the air bubbles, which do not produce any signal, tend to shift a bit in location and size during the experiments. In addition, due to imperfect orthogonally of the gradient coils in the present setup, when one employs different values of $\tau$ (Fig. 3), the image planes shift slightly, a fact that also tends to distort a bit the images one with respect to the other.

In general, as one steps out the parameter $\tau$, the amplitude of the image decreases exponentially with characteristic time

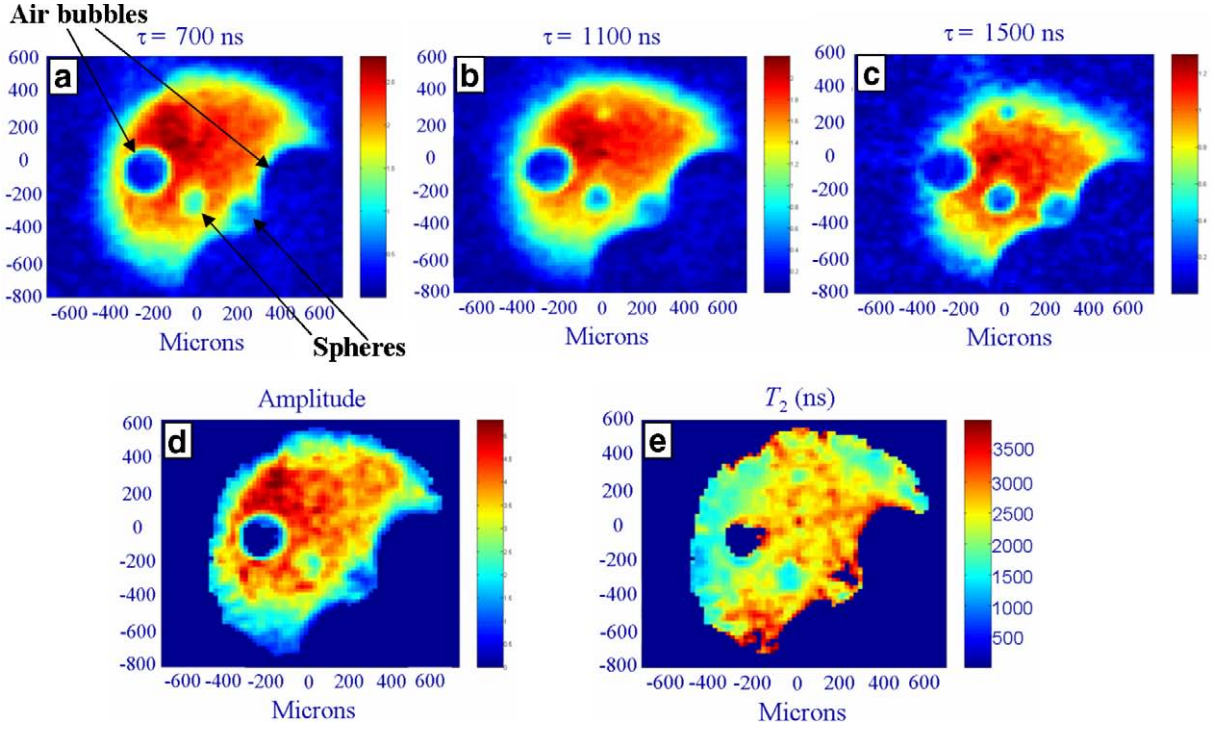


Fig. 10. ESRM experimental results. (a) A 2D cut of the 3D image, showing the central plane of the imaged spheres and the air bubbles, where no signal is obtained, marked with arrows (Fig. 7). A small air bubble is apparent on the left and a large bubble dominates the entire lower right part of the image. The image was obtained with $\tau$=700 ns (Fig. 3). The vertical color bar represents the relative pixel ESR signal in arbitrary units. (b) The same as a, but for $\tau$=1100 ns. (c) The same as a, but for $\tau$=1500 ns. (d) Amplitude image obtained from the images taken at different $\tau$ (see text). (e) Spin–spin relaxation time, $T_2$, image obtained voxel-like from the images taken at different $\tau$ (see text). In d and e, the voxel signal or $T_2$ values are assumed to be 0 if the amplitude in that voxel is below a certain threshold. This enables one to avoid the presentation of unreliable data.

$T_2$ (also called the spin–spin relaxation time). If the sample is inhomogeneous in terms of its ESR properties, this may result in an inhomogeneous spatially resolved $T_2$. In order to extract the spatially resolved $T_2$ parameter from the raw image data, we extrapolate the spatially resolved echo amplitude to $\tau=0$, based on the data gathered for each voxel at the three different values of $\tau$. This extrapolation provides us first with the spin concentration for each voxel (termed "amplitude image" in Fig. 10d), which is the signal originating from the voxel without any effects from relaxation. In addition, we obtain the decay time, $T_2$ of each individual voxel (Fig. 10e). In other words, we perform a fit to a simple exponential decay curve for each voxel, based on the voxel signal for the three measured $\tau$ values, to determine the amplitude of the exponent and its decay constant. From the measured data, it is evident that only one of the spheres (the left one) absorbed some water in the time scale of the experiment, while the other one (on the right) for some unknown reason did not absorb much water and thus does not exhibit any substantial ESR signal (cf. Fig. 8d). The calculated amplitude image shows substantial signal from the left sphere, although it is still ~50% smaller than the surrounding water. This signal reduction is undoubtedly due to the release matrix (PLGA) volume, which obviously does not contain any radicals. The calculated $T_2$ image shows that the radicals in the left sphere have a shorter $T_2$ of ~1400 ns, compared to a $T_2$ of ~3100 ns for trityl in the water around it. The phenomenon of different $T_2$ inside and outside the sphere is also evident through a qualitative examination of the raw image data, which show increased contrast between the sphere and the solution around it, for larger values of $\tau$. The shorter $T_2$ inside the sphere corresponds well with the CW measurements (Fig. 8), since shorter $T_2$ implies larger CW linewidth.

It is well known that even a small amount of PEG solvated in water causes a relatively large increase in the solution viscosity over that of pure water [41]. Another known mechanism for increased viscosity is due to surface–water interaction in small pores [42]. It is also known that the solvent viscosity strongly affects the relaxation time $T_2$ of the trityl radical [38]. It thus seems reasonable to conclude that the reduction in $T_2$ from within the sphere is due to increased viscosity in the pores where the water/PEG/trityl solution contributes to the measured signal. On a more quantitative level, Owenius et al. [38] have measured at 9 GHz a reduction in $T_2$ from 9.1 μs to 1.8 μs, for 0.2 mM trityl solution in pure water vs. water with 50% glycerol as a solvent (which has a viscosity of ~5.25 cP at room temperature [43]). We, on the other hand, have measured at 17.2 GHz a $T_2$ of 3.3 μs, for 1 mM trityl water solution, and $T_2$'s of 2.2 and 1 μs, for 40% and 70% glycerol 1 mM trityl solution, respectively (with viscosity of 3.42 and 18.6 cP, respectively) [22]. These values are more relevant to the present ESRM experiments (since we employed a release solution with 1 mM trityl and we worked at 16 GHz). These numbers suggest that the inner pore viscosity was ~10 cP in the measurements described above (Fig. 10). In addition to the reduction in $T_2$ (which corresponds to larger linewidth), we were able to identify with the bulk CW measurements a slight change in $g$ factor from within the spheres (Fig. 8b). This may suggest that the trityl molecule is bound either to the release matrix (PLGA) or to the PEG. In such a case, the decrease in $T_2$ value may not be due to increased viscosity, but as a consequence of this binding. Our present ESRM capabilities, employing this specific trityl radical probe, cannot provide a clear cut answer to these two possibilities (i.e. increased viscosity and/or binding to the matrix). Nevertheless, in the near future, the use of pulsed field gradients, in a similar manner to NMR [9], combined with full spectral spatial imaging (which provides the spectrum at each voxel), would enable one to directly measure the self-diffusion coefficient and extract the rotational correlation time of the radical. This would enable the separation and positive identification of mechanisms such as diffusion change (due to varying viscosity) vs. rotational correlation times variation (due to binding), which both affect $T_2$ in a similar manner. An additional plan for future work would be to directly compare LSCF and ESRM by employing the same drug molecule first labeled with a spin label (for the ESRM) and subsequently with a fluorescence probe (for LSCF).

## 4. Conclusions

ESRM is an emerging technique with several potential applications in the fields of biophysics and materials science. In the context of controlled release research, ESRM that employs spin-labeled drug molecules has the potential of providing vital information from within the release matrix with micron-scale resolution. Data such as drug concentration, self-diffusion tensor, rotational correlation time, molecular conformation and pH may be imaged in-situ in a 3D manner and may also be correlated with in-vivo large-scale ESR imaging measurements. In the present work, an initial step has been made towards realizing these capabilities. The experimental results demonstrate that high resolution images of very small geometries of relevance (e.g. ~100 μm biodegradable microspheres) can be obtained with sufficient SNR. The ESR images exhibit substantial changes in the properties of the trityl free radical when situated inside and outside the microsphere, which are attributed to possible elevated viscosity inside the sphere or radical binding to the matrix. Further efforts are currently being undertaken to improve upon the current limitation of the system such as sample preparation procedure, enhancement of the image resolution and SNR (mainly by employing higher magnetic fields), adding the capability to directly image $\boldsymbol{D}$ through the pulsed field gradient method and enabling full spectral–spatial acquisition. These developments, combined with the use of more common spin probes, such as nitroxides, should provide fine details about the underlining physical conditions in the matrix in a manner similar to the capabilities of bulk ESR measurements [30].

## Acknowledgments

We are grateful for Dr. Lars-G. Wistrand from Nycomed Innovations in Sweden for providing us with the trityl radical.

This research was supported by grant #P41RR016292 from NIH/NCRR (AB and JHF).

## References


[1] H.M. Wong, J.J. Wang, C.H. Wang, In vitro sustained release of human immunoglobulin G from biodegradable microspheres, Ind. Eng. Chem. Res. 40 (2001) 933–948.

[2] S.P. Rigby, C.F. Van der Walle, J.H. Raistrick, Determining drug spatial distribution within controlled delivery tablets using MFX imaging, J. Control. Release 96 (2004) 97–100.

[3] K. Remaut, B. Lucas, K. Braeckmans, N.N. Sanders, S.C. De Smedt, J. Demeester, FRET-FCS as a tool to evaluate the stability of oligonucleotide drugs after intracellular delivery, J. Control. Release 103 (2005) 259–271.

[4] K. Mader, S. Nitschke, R. Stosser, H.H. Borchert, A. Domb, Non-destructive and localized assessment of acidic microenvironments inside biodegradable polyanhydrides by spectral spatial electron paramagnetic resonance imaging, Polymer 38 (1997) 4785–4794.

[5] L. Li, S.P. Schwendeman, Mapping neutral microclimate pH in PLGA microspheres, J. Control. Release 101 (2005) 163–173.

[6] C.D. Melia, A.R. Rajabi-Siahboomi, R.W. Bowtell, Magnetic resonance imaging of controlled release pharmaceutical dosage forms, Pharm. Sci. Technol. Today 1 (1998) 32–39.

[7] S.G. Kazarian, K.L.A. Chan, "Chemical photography" of drug release, Macromolecules 36 (2003) 9866–9872.

[8] C.A. Coutts-Lendon, N.A. Wright, E.V. Mieso, J.L. Koenig, The use of FT-IR imaging as an analytical tool for the characterization of drug delivery systems, J. Control. Release 93 (2003) 223–248.

[9] P.T. Callaghan, Principles of Nuclear Magnetic Resonance Microscopy, Oxford University Press, Oxford, 1991.

[10] P. Glover, P. Mansfield, Limits to magnetic resonance microscopy, Rep. Prog. Phys. 65 (2002) 1489–1511.

[11] K. Braeckmans, L. Peeters, N.N. Sanders, S.C. De Smedt, J. Demeester, Three-dimensional fluorescence recovery after photobleaching with the confocal scanning laser microscope, Biophys. J. 85 (2003) 2240–2252.

[12] A.L. Lee, A.J. Wand, Assessing potential bias in the determination of rotational correlation times of proteins by NMR relaxation, J. Biomol. NMR 13 (1999) 101–112.

[13] A.H.A. Clayton, Q.S. Hanley, D.J. Arndt-Jovin, V. Subramaniam, T.M. Jovin, Dynamic fluorescence anisotropy imaging microscopy in the frequency domain (rFLIM), Biophys. J. 83 (2002) 1631–1649.

[14] F.W. Koehler, E. Lee, L.H. Kidder, E.N. Lewis, Near infrared spectroscopy: the practical chemical imaging solution, Spectrosc. Eur. 14 (2002) 12–19.

[15] S. Capancioni, K. Schwach-Abdellaoui, W. Kloeti, W. Herrmann, H. Brosig, H.H. Borchert, J. Heller, R. Gurny, In vitro monitoring of poly (ortho ester) degradation by electron paramagnetic resonance imaging, Macromolecules 36 (2003) 6135–6141.

[16] . K. Mader, G. Bacic, A. Domb, O. Elmalak, R. Langer, H.M. Swartz, Noninvasive in vivo monitoring of drug release and polymer erosion from biodegradable polymers by EPR spectroscopy and NMR imaging, J. Pharm. Sci. 86 (1997) 126–134.

[17] N. Kocherginsky, H.M. Swartz, Nitroxide Spin Labels: Reactions in Biology and Chemistry, CRC Press, Boca Raton, FL, 1995.

[18] S.P. Gabbita, R. Subramaniam, F. Allouch, J.M. Carney, D.A. Butterfield, Effects of mitochondrial respiratory stimulation on membrane lipids and proteins: an electron paramagnetic resonance investigation, Biochim. Biophys. Acta-Biomembranes 1372 (1998) 163–173.

[19] A. Wrobel, J. Gomulkiewicz, Electron paramagnetic resonance studies of membrane fluidity in ozone-treated erythrocytes and liposomes, Biochem. Mol. Biol. Int. 47 (1999) 99–105.

[20] C.G. Pitt, J. Wang, S.S. Shah, R. Sik, C.F. Chignell, ESR spectroscopy as a probe of the morphology of hydrogels and polymer–polymer blends, Macromolecules 26 (1993) 2159–2164.

[21] A. Brunner, K. Mader, A. Gopferich, pH and osmotic pressure inside biodegradable microspheres during erosion, Pharm. Res. 16 (1999) 847–853.

[22] A. Blank, C.R. Dunnam, P.P. Borbat, J.H. Freed, High resolution electron spin resonance microscopy, J. Magn. Reson. 165 (2003) 116–127.

[23] A. Blank, C.R. Dunnam, P.P. Borbat, J.H. Freed, 3D continuous wave electron spin resonance microscope, Rev. Sci. Instrum. 75 (2004) 3050–3061.

[24] A. Blank, C.R. Dunnam, P.P. Borbat, J.H. Freed, Pulsed three-dimensional electron spin resonance microscopy, Appl. Phys. Lett. 85 (2004) 5430–5432.

[25] C.P. Poole, Electron Spin Resonance: A Comprehensive Treatise on Experimental Techniques, 2nd ed.Wiley, New York, 1983.

[26] J.P. Hornak, J.K. Moscicki, D.J. Schneider, J.H. Freed, Diffusion-coefficients in anisotropic fluids by electron-spin-resonance imaging of concentration profiles, J. Chem. Phys. 84 (1986) 3387–3395.

[27] J.K. Moscicki, Y.K. Shin, J.H. Freed, Dynamic imaging of diffusion by ESR, J. Magn. Reson. 84 (1989) 554–572.

[28] A. Feintuch, T. Tashma, A. Grayevsky, J. Gmeiner, E. Dormann, N. Kaplan, Combined *k*-space *q*-space pulsed ESR imaging: mapping of restricted diffusion in (FA)(2)PF6, J. Magn. Reson. 157 (2002) 69–73.

[29] A. Blank, E. Stavitski, H. Levanon, F. Gubaydullin, Transparent miniature dielectric resonator for electron paramagnetic resonance experiments, Rev. Sci. Instrum. 74 (2003) 2853–2859.

[30] P.P. Borbat, A.J. Costa-Filho, K.A. Earle, J.K. Moscicki, J.H. Freed, Electron spin resonance in studies of membranes and proteins, Science 291 (2001) 266–269.

[31] J.H. Freed, New technologies in electron spin resonance, Annu. Rev. Phys. Chem. 51 (2000) 655–689.

[32] M.S. Conradi, A.N. Garroway, D.G. Cory, J.B. Miller, Generation of short, intense gradient pulses, J. Magn. Reson. 94 (1991) 370–375.

[33] K.J. Liu, P. Gast, M. Moussavi, S.W. Norby, N. Vahidi, T. Walczak, M. Wu, H.M. Swartz, Lithium phthalocyanine—a probe for electron-paramagnetic-resonance oximetry in viable biological-systems, Proc. Natl. Acad. Sci. U. S. A. 90 (1993) 5438–5442.

[34] P.K. Naraharisetti, MSc Thesis, Local administration in osteomyelitis by drug encapsulated polymer beads, in the Department of Chemical and Biomolecular Engineering, National University of Singapore: Singapore, 2003.

[35] P.K. Naraharisetti, M.D.N. Lew, Y.C. Fu, D.J. Lee, C.H. Wang, Gentamicin-loaded discs and microspheres and their modifications: characterization and in vitro release, J. Control. Release 102 (2005) 345–359.

[36] J.H. Ardenkjaer-Larsen, I. Laursen, I. Leunbach, G. Ehnholm, L.G. Wistrand, J.S. Petersson, K. Golman, EPR and DNP properties of certain novel single electron contrast agents intended for oximetric imaging, J. Magn. Reson. 133 (1998) 1–12.

[37] L. Yong, J. Harbridge, R.W. Quine, G.A. Rinard, S.S. Eaton, G.R. Eaton, C. Mailer, E. Barth, H.J. Halpern, Electron spin relaxation of triarylmethyl radicals in fluid solution, J. Magn. Reson. 152 (2001) 156–161.

[38] R. Owenius, G.R. Eaton, S.S. Eaton, Frequency (250 MHz to 9.2 GHz) and viscosity dependence of electron spin relaxation of triarylmethyl radicals at room temperature, J. Magn. Reson. 172 (2005) 168–175.

[39] R.P. Pandian, N.L. Parinandi, G. Ilangovan, J.L. Zweier, P. Kuppusamy, Novel particulate spin probe for targeted determination of oxygen in cells and tissues, Free Radic. Biol. Med. 35 (2003) 1138–1148.

[40] R.P. Pandian, P. Kuppusamy, Lithiated phthalocyanines: a new class of crystalline paramagnetic probes for targeted cellular oximetry and imaging by EPR spectroscopy, Biophys. J. 86 (2004) 191a.

[41] C.B. Goncalves, N. Trevisan, A.J.A. Meirelles, Kinematic viscosity of systems containing polyethylene glycol plus salt plus water at 298.2 K, J. Chem. Eng. Data 50 (2005) 177–181.

[42] R. Kimmich, S. Stapf, A.I. Maklakov, V.D. Skirda, E.V. Khozina, Self-diffusion in fluids in porous glass: confinement by pores and liquid adsorption layers, Magn. Reson. Imaging 14 (1996) 793–797.

[43] P.N. Shankar, M. Kumar, Experimental-determination of the kinematic viscosity of glycerol water mixtures, Proc. R. Soc. Lond., Ser. A 444 (1994) 573–581.